Very low velocity ion slowing down in binary ionic mixtures: Charge- and mass-asymmetry effects

Patrice Fromy

Direction de l'Informatique, Université Paris XI, 91405 Orsay, France

Bekbolat Tashev

Department of Physics, Kazakh National University, Almaty 480012, Kazakhstan

Claude Deutsch

LPGP (UMR-CNRS 8578), Université Paris XI, 91405 Orsay, France

A binary ionic mixture (BIM) in dense and hot plasmas of specific concern for inertial confinement fusion and white dwarf crust is considered as a target for incoming light ions with a velocity smaller than the thermal electron one. The given target stopping power, mostly BIM monitored, is specifically studied in terms of charge and mass asymmetry in its ionic component. The classical plasma target is worked out within a dielectric framework, and scanned with respect to density, temperature, and BIM composition.

I. INTRODUCTION

Low velocity ion slowing down (LVISD) has been for a long time a very important topic featuring the last stage of the ion-dense target interaction. Initially, the given targets were taken as cold ones, with projectile ion velocity V_p currently contrasted to orbital velocities of electrons bound to that target [1]. Here we address the LVISD issues in fully ionized plasmas built on binary ionic mixtures (BIM) such as the deuterium-tritium (DT) BIM of current interest in thermonuclear fusion research. In particular, the control of the resulting alpha particles, is of paramount significance in the conduct of inertial fusion energy (IFE) as well as magnetic fusion energy (MFE) senarii to economical success. The given control demands a basic and fundamental understanding of the α's LVISD, which, produced at 3.5 MeV, lose most of their energy to the surrounding plasma with a $V_p \leq V_{\text{the}}$ electron thermal velocity. Similar considerations apply to the present U.S. program devoted to the production of warm dense matter with low velocity ions linearly accelerated, and fully stopped in complex and initially cold targets [2]. Here, the accelerator parameters are tuned so that the largest ion projectile energy loss takes in the vicinity of the Bragg peak, near the end of range [3]. In this latter case, the goal is to produce plasmas with a density between $1/10$ and 10 times solid density, with a temperature below 10 eV, in order to probe the whole scale of strongly coupled ions and arbitrary degeneracy in the neutralizing electron fluid.

Considering the BIM target with neutralizing electrons, in a dielectric framework, the ion beam-target interaction is essentially qualified through a dimensionless ratio of average collision parameter $\langle bo \rangle$ and dynamical screening length, λ, given as [4]

$$\frac{\langle bo \rangle}{\lambda} = \frac{|Z_{\text{eft}}|}{N_D} \cdot \frac{1}{3(1 + \frac{V_p^2}{V_{\text{the}}^2})^{3/2}},$$

maximized at $V_p = 0$ with $N_D = n_e \lambda_D^3$, in terms of target electron density n_e and Debye length $\lambda_D(\text{cm}) = 743\sqrt{\frac{T(\text{eV})}{n_e(\text{cm}^{-3})}}$.

In the sequel, we shall restrict to weakly coupled plasma targets with $N_D \gg 1$, which nonetheless encompass most plasmas of IFE and MFE interest. We shall work out LVISD with V_p alternatively scaled to V_{the} and V_{thi}, ion thermal velocity, in order to probe its very low V_p specific features, arising mostly from Coulomb interaction between incoming ion projectile and target BIM.

The given ion beams are taken dynamically uncorrelated.

The remaining part of this work is structured as follows. Section II deals with LVISD technicalities considered within dielectric formalism grounded on the Fried-Conte [5] classical formulation used additively for the neutralizing electrons and BIM, as well.

Then, we develop a parameter study based on increasing values of charge Z_2/Z_1 and mass M_2/M_1 ratios for the target BIM built on pointlike classical ions (Z_1, M_1) and (Z_2, M_2). Section III is thus first devoted to the nearly symmetric DT fuel. Section IV details asymmetries introduced by arbitrary M_2/M_1 at fixes Z_2/Z_1. From Sec. V, we investigate several BIM with $Z_2/Z_1 > 1$, of considerable interest for thermonuclear fusion and astrophysics as well. The specificities of neutral BIM including antiprotons (pbars) are briefly sketched in Sec. VI. Outlooks are offered in Sec. VII.

II. DIELECTRIC STOPPING FORMALISM

We modelize dense and mostly hot plasma targets as binary ionic mixtures (BIM) of pointlike and classical ions (M_1, Z_1) and (M_2, Z_2), neutralized by a classical electron fluid described within the framework of the Fried-Conte dielectric function [5].

In such an approach, it appears useful to work with the overall dielectric function

$$\varepsilon(\vec{k}, \omega) = 1 + \frac{1}{k^2}\left[W\left(\frac{\omega}{k}\right) + W\left(\sqrt{M_1}\frac{\omega}{k}\right) + W\left(\sqrt{M_2}\frac{\omega}{k}\right)\right] \tag{1}$$

with the usual Fried-Conte dispersion function $W(\text{Im}\varsigma \geq 0)$

$$W(\varsigma) = \frac{1}{\sqrt{2\pi}} \lim_{\nu \to 0+} \int_{-\infty}^{\infty} dx \frac{xe^{-x^2/2}}{x - \varsigma - i\nu} \tag{2}$$

and $X(\zeta) = \text{Re } W(\zeta)$, $Y(\zeta) = \text{Im } W(\zeta)$. Generalizing linearly through expression (2), the standard one-component stopping quadrature [6,7]

$$-\left[\frac{dE}{dx}\right] = \frac{Z^2 N_D}{(2\pi)^2} \int_0^{k_{\max}} dk k^3 \int_{-1}^{+1} d\mu \\ \times \frac{\mu Y(\mu V_p)}{[k^2 + X(\mu V_p)]^2 + Y^2(\mu V_p)} \tag{3}$$

with $Z = Z_{\text{eff}}/N_D$, where Z_{eff} denotes the projectile effective charge at velocity v_p, $N_D = n_e \lambda_{\text{De}}^3$ in terms of target electron density and corresponding Debye length. In the sequel, v_p will be scaled by $v_{\text{the}} = \sqrt{k_B T/m_e}$, thermal electron velocity with T, thermalized target temperature. In Eq. (3), we have to pay attention to the selection of maximum cutoff $k_{\max}$, taking into account quantum effects diffraction ($k_B T \gtrsim 1$ Ry) in a high temperature plasma. So, one explicits [6,7]

$$k_{\max} = \min\left(\frac{m(V_p^2 + V_{\text{the}}^2)}{Z_{\text{eff}} e^2}, \frac{2m\sqrt{V_p^2 + V_{\text{the}}^2}}{\hbar}\right) \\ = \min\left(\frac{4\pi}{Z}(v_p^2 + 1), 8\pi\sqrt{2}N_D \frac{\alpha c}{V_{\text{the}}}\sqrt{v_p^2 + 1}\right), \tag{4}$$

where v_p is now dimensionless on the second line on the right-hand side. $\alpha = 1/137$ is the fine structure constant, and c is light velocity. In this regard, it should be noticed that the occurrence of quantum diffraction $k_{\max}$ is restricted to the electron fluid component of the target. The corresponding BIM will always appear as pointlike classical, as long as one restricts to the velocity range $V_{\text{thi}} \leq V_p \leq V_{\text{the}}$. In adapting Eq. (3) to BIM stopping, it proves convenient to introduce the relative ion concentration of species 1, i.e.,

$$\alpha = \frac{N_1}{N_1 + N_2}, \tag{5}$$

in terms of ion number N_i with $i = 1, 2$, in target plasma, so that BIM densities,

$$n_1 = \frac{n_e \alpha}{\bar{Z}}, \qquad n_2 = \frac{n_e(1-\alpha)}{\bar{Z}}, \qquad \bar{Z} = Z_1 \alpha + Z_2(1-\alpha), \tag{6}$$

are straightforwardly expressed in terms of electron density n_e.

Then, we can estimate the stopping contributions of every target component: electron (0), ion 1, and ion 2 as follows:

$$-\frac{dE_0}{dx} = C_0 \int_0^{k_{\max 0}} dk k^3 \int_{-1}^{+1} d\mu \frac{\mu Y[\mu v_p]}{D[k, \mu v_p]}, \tag{7a}$$

$$-\frac{dE_1}{dx} = C_1 \int_0^{k_{\max 1}} dk k^3 \int_{-1}^{+1} d\mu \frac{\mu Y[\sqrt{M_1}\mu v_p]}{D[k, \mu v_p]}, \tag{7b}$$

$$-\frac{dE_2}{dx} = C_2 \int_0^{k_{\max 2}} dk k^3 \int_{-1}^{+1} d\mu \frac{\mu Y[\sqrt{M_2}\mu v_p]}{D[k, \mu v_p]}, \tag{7c}$$

where

$$D[k, \mu v_p] = (k^2 + X[\mu_p v_p] + X[\sqrt{M_1}\mu v_p] \\ + X[\sqrt{M_2}\mu v_p])^2 + (Y[\mu v_p] \\ + Y[\sqrt{M_1}\mu v_p] + Y[\sqrt{M_2}\mu v_p])^2, \tag{8}$$

$$C_0 = \frac{k_B T Z_{\text{eff}}^2}{4\pi^2 n_e \lambda_D^4}, \tag{9a}$$

$$C_1 = \frac{C_0 Z_1^4 \alpha}{\bar{Z}}, \tag{9b}$$

$$C_2 = \frac{C_0 Z_2^4 (1 - \alpha)}{\bar{Z}}, \tag{9c}$$

altogether with

$$k_{\max 0} = \min\left(k_{\max 0}^1 = n_e \lambda_D^3 \frac{4\pi(v_p^2 + 1)}{Z_{\text{eff}}}, \\ 185.73 n_e \lambda_D^3 \sqrt{\frac{v_p^2 + 1}{T(\text{eV})}}\right), \tag{10a}$$

$$k_{\max 1} = \frac{k_{\max 0}^1}{Z_1^3}\left(\frac{\bar{Z}}{\alpha}\right)^{1/2}, \tag{10b}$$

$$k_{\max 2} = \frac{k_{\max 0}^1}{Z_2^3}\left(\frac{\bar{Z}}{1-\alpha}\right)^{1/2}. \tag{10c}$$

Expressions (7a)–(7c) are in $k_B T/\lambda_D$, with the Debye screening length λ_D, respectively, adapted to electron, ion 1, and ion 2. V_p is in V_{the}.

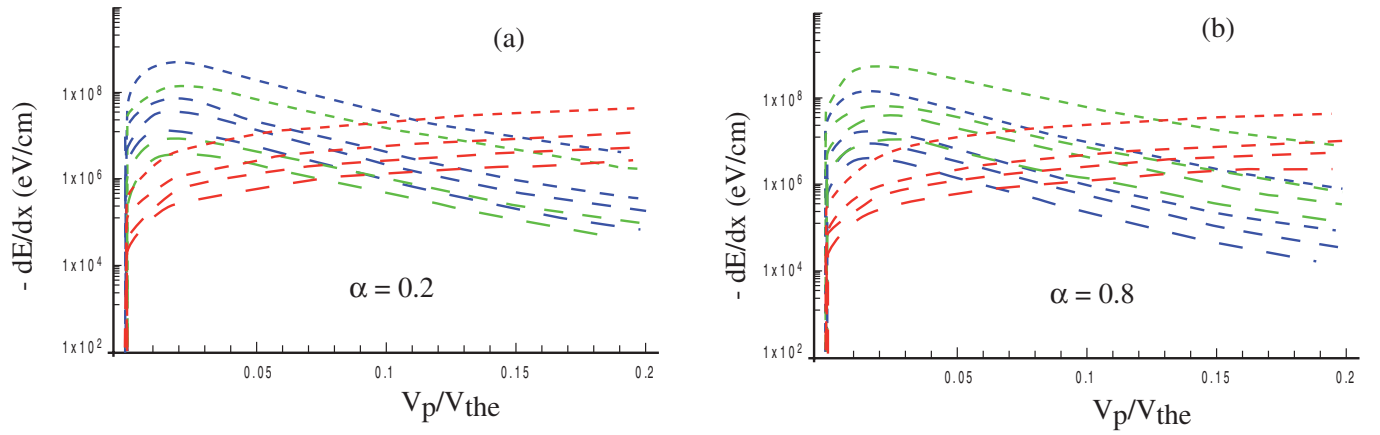FIG. 1. (Color) Proton particle projectile in a deuterium-tritium BIM with $n_e = 10^{23}$ e-cm^{-3} and temperatures = (- - - - - -) 100 eV, (- - - - -) 1 keV, (- - - ·) 2 keV, and (— — —) 5 keV with D^+ relative proportion: (a) $\alpha = 0.2$ and (b) $\alpha = 0.8$. Dark gray (red) refers to electron stopping, light gray (green) to D^+ stopping, and black (blue) denotes T^+ stopping, $-dE/dx$ (eV/cm) in terms of V_p/V_{the}.

The target electron cutoff estimate (10a) shows that corresponding $\hbar \neq 0$ corrections should be included for equilibrium temperatures $T = T_e = T_i \geq 110$ eV. Target ion slowing down contributions remain classical as long as $T \leq 200 \, (M_i/1836)$ keV, provided the right-hand side of Eqs. (10b) and (10c) replaces $v_p^2 + 1$ by $M_1 v_p^2 + 1$ and $M_2 v_p^2 + 1$, respectively, with V_p in V_{the}. When target ions enter the $\hbar \neq 0$ regime, the right-hand term within brackets in Eq. (10a) becomes $7930 \sqrt{(v_p^2 + 1)} \frac{M_i}{1836 \, T(eV)}$ for ion species i.

For $k_{max} \gg 1$, it appears convenient to extend a previous analytic LVISD expression [6], to the present BIM situation with

$$ -\frac{dE}{dx} = \frac{Z^2 N_D}{12\pi\sqrt{2\pi}} \frac{V_p}{V_{the}} \sqrt{\bar{M}} \, \ell n \left[\bar{M}^2 \frac{32\pi^2}{Z2} \right], \qquad (11) $$

where $Z = Z_{eff}/(n_e \lambda_D^3)$ and $\bar{M} = \alpha M_1 + (1 - \alpha) M_2$

III. QUASISYMMETRIC BIM

We begin our analysis with the quasisymmetric BIM D^+-T^+, of paramount significance in present thermonuclear fusion research [8]. Figure 1 features rather convincingly the expected quasisymmetric behavior $\alpha \leftrightarrow 1-\alpha$, for the proton projectiles low ion velocity slowing down, for a rather dense plasma target of inertial fusion energy (IFE) concern [8] with $n_e = 10^{23}$ e-cm^{-3} and a rather wide temperature range $T(eV)\varepsilon[10, 5000]$. Stopping data $-dE/dx$ are given in $\frac{T(eV)}{\lambda_D(cm)}$, with $\lambda_D(cm) = 743 \sqrt{\frac{T(eV)}{n_e(cm^{-3})}}$, target electron Debye length, in terms of V_p/V_{the}. BIM stopping contributions, light gray (green) for D^+ stopping, and black (blue) for T^+ stopping, display mostly a negative
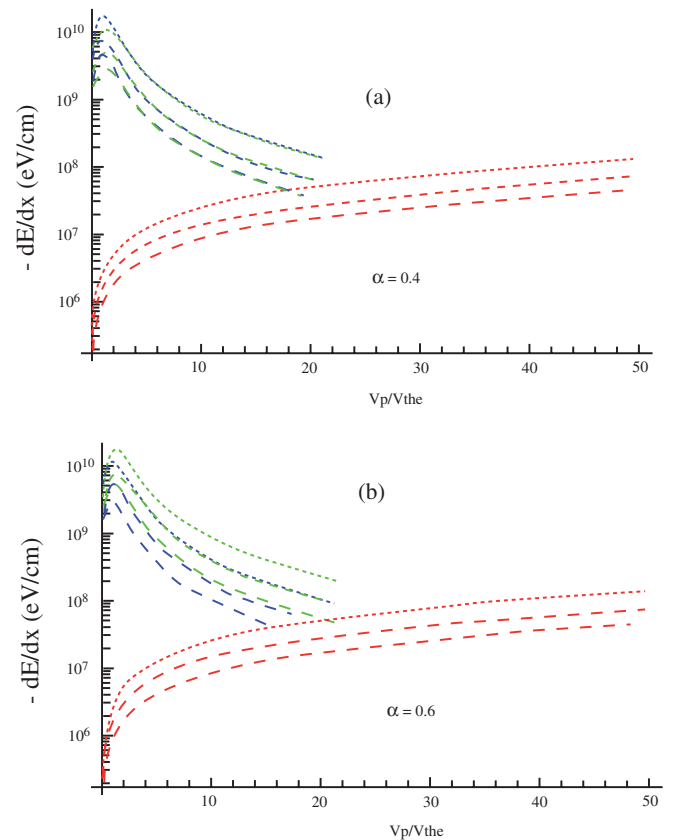

FIG. 2. (Color) Proton particle projectile in a deuterium-tritium BIM with $n_e = 10^{26}$ e cm^{-3} and temperatures = (· · · · · · · · ·) 1 keV, (- - - - -) 2 keV, (— — —) 10 keV with D^+ relative proportion: (a) $\alpha = 0.4$ and (b) $\alpha = 0.6$. Dark gray (red) refers to electron stopping, light gray (green) to D^+ stopping, and black (blue) denotes T^+ stopping, $-dE/dx$ (eV/cm) in terms of V_p/V_{the}.
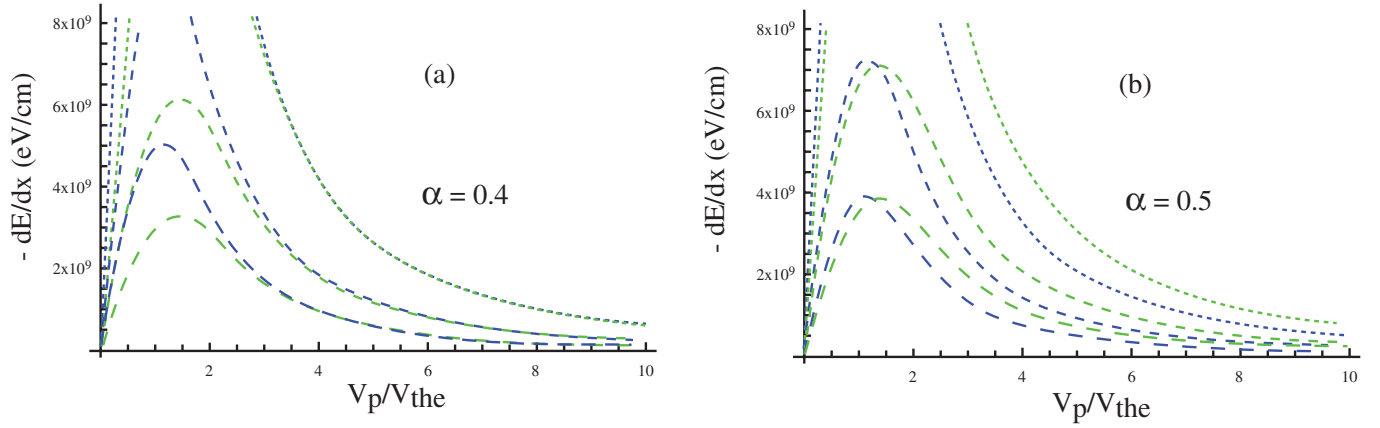
FIG. 3. (Color) Proton particle projectile in a deuterium-tritium BIM with $n_e = 10^{26}$ e cm^{-3} and temperatures = ($\cdots\cdots$) 1 keV, ($- - - - -$) 2 keV, ($- \ - \ - \ -$) 10 keV, with D^+ relative proportion: (a) $\alpha = 0.4$ and (b) $\alpha = 0.5$. Dark gray (red) refers to electron stopping, light gray (green) to D^+ stopping, and black (blue) denotes T^+ stopping, $-dE/dx$ (eV/cm) in terms of V_p/V_{the}.

slope, and cross the dark gray (red) electron-stopping contribution for $0.05 \leq V_p/V_{\text{the}} \leq 0.2$, with an increasing one.

It should also be appreciated that the least abundant i component (smallest α) crosses the e contribution at lower V_p values.

Best matching between D^+—and T^+—curves occurs around $\alpha = 0.4$, for $V_p/V_{\text{the}} \geq 0.1$. At $\alpha = 0.5$, the lightest ion D^+ provides a stopping contribution (SC) slightly above the T^+ one, in log scale, due to the modest M_{D^+}-M_{T^+} mass difference. Switching the above exploration to the core plasma envisioned in the fast ignition scenario for IFE, one witnesses the pertaining LVISD quantities in Fig. 2 for $n_e = 10^{26}$ e-cm^{-3} with $T(\text{keV}) = 2$, 5, and 10, in terms of $V_{\text{th1}} = V_{\text{the}}/60$, on a range equivalent to that of Fig. 1.

Again an excellent agreement between D^+—and T^+—stopping is observed at $V_p/V_{\text{thi}} \geq 1$, i.e. $= V_p/V_{\text{the}} \geq 0.016$ (Fig. 1).

Figures 1 and 2 basically feature a linear in $V_p \ll V_{\text{the}}$ e stopping, contrasted to strongly asymmetric bell-shaped i-stopping curves, with a Bethe-like decay $\sim V_p^{-2}$ for $V_p \geq V_{\text{thi}}$. The given bell shapes turn much more symmetrical with $-dE/dx$ in linear scale (Fig. 3), on a reduced $V_p/V_{\text{thi}} \leq 10$ range. Then, the e stopping becomes hardly noticeable, on the V_p axis. The optimized matching at $\alpha = 0.4$ between D^+—and T^+—stopping is also very accurately documented.

IV. MASS ASYMMETRY ($Z_1 = Z_2 = 1$, $M_2/M_1 \gg 1$)

The above D^+-T^+ captions (Figs. 1–3) dedicated to BIM with $M_1/M_2 = 2/3$ feature parallel stopping contributions with no crossing, except with the electron one. Here, we enlarge considerably the M_2/M_1 ratio while keeping same charge unity on H^+ and U_{238}^+ (Figs. 4 and 5), in dense IFE plasmas with $n_e = 10^{23}$ e-cm^{-3} and $T(\text{keV}) = 1$, 5, and 10, submitted to proton projectiles.

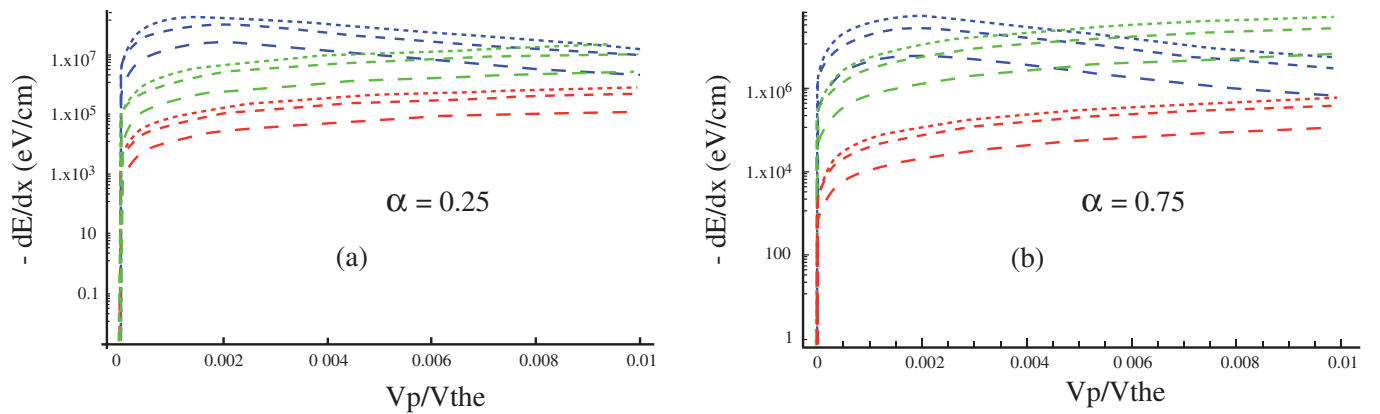FIG. 4. (Color) Proton particle projectile in a proton-U$_{238}^+$ BIM with $n_e = 10^{26}$ e cm^{-3} and temperatures = ($\cdots\cdots$) 1 keV, ($- - - - - - -$) 5 keV, ($- \ - \ - \ -$) 10 keV, with H^+ relative proportion: (a) $\alpha = 0.25$, (b) $\alpha = 0.75$. Dark gray (red) refers to electron stopping, light gray (green) to D^+ stopping, and black (blue) denotes T^+ stopping, $-dE/dx$ (eV/cm) in terms of V_p/V_{the}.
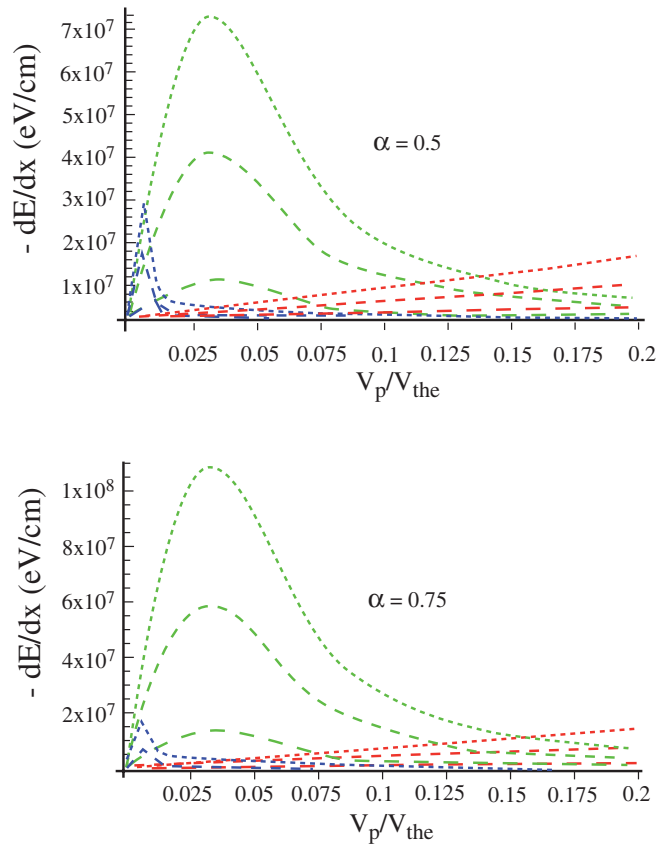
FIG. 5. (Color) Proton stopping in H^+-U_{238}^+ BIM in terms of V_p/V_{the}. $n_e = 10^{23}$ e cm^{-3}. Alpha denotes proton concentration in BIM. T(eV) = ($\cdots\cdots$) 500, ($-\cdot-\cdot-\cdot$) 1000, and ($----$) 5000. Dark gray (red) pertains to e stopping, light gray (green) to H^+ stopping, and black (blue) to H^+ stopping. U_{238}^+ stopping.

Then, the U_{238}^+ (blue stopping contribution crosses the H^+ green) at $V_p/V_{the} \lesssim 0.01$.

Such a large M_2/M_1 ratio induces a strong localization of the heaviest ion stopping efficiency very close to very small ion projectile V_p values. Figures 4 and 5 clearly demonstrate that as soon as $\alpha \gtrsim 0, 5$, the heaviest U_{238}^+ stopping contribution can be quantitatively neglected in front of the proton one. The latter (Fig. 5) extends over the full V_p range, up to a crossing area with electron linear curves. This phenomenon highlights a much easier energy transfer between incoming proton projectile and target protons than with the hardly mobile U_{238}^+ ions. Very similar behaviors are featured by the same BIM immersed in much more dilute plasmas of magnetic fusion energy (MFE) concern with $n_e = 10^{14}$ e-cm^{-3}.

V. CHARGE ASYMMETRY

A. Proton-boron 11 ($Z_2/Z_1 = 5$, $M_2/M_1 = 10.81$) BIM

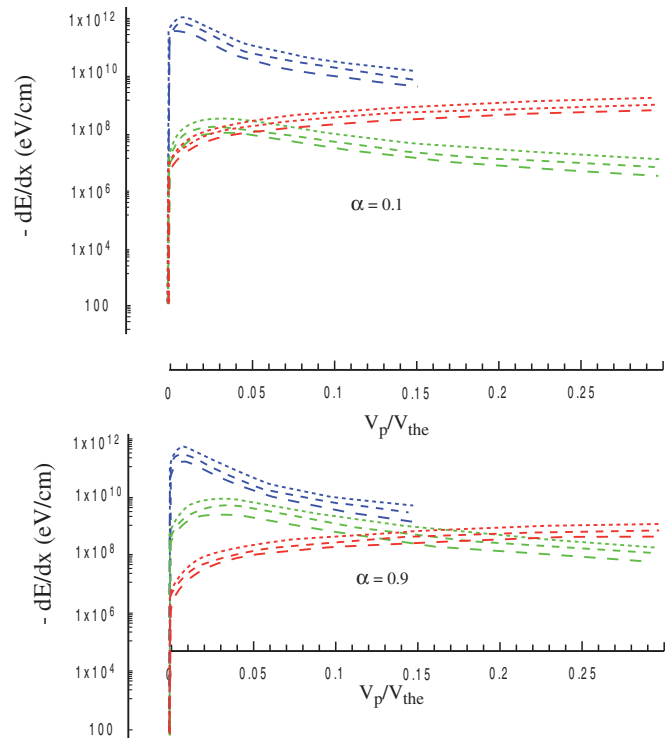Switching interest to BIM with asymmetric charge distribution, we first pay attention to a specific fuel of alter-

FIG. 6. (Color) Proton stopping in H^+-B^{5+} BIM in terms of V_p/V_{the} $n_e = 10^{25}$ e cm^{-3}. Alpha denotes proton concentration in BIM. T(eV) = ($\cdots\cdots$) 500, ($------$) 1000, and ($----$) 2000. Dark gray (red) pertains to e stopping, light gray (green) to H^+ stopping, and black (blue) to B^{5+} stopping.

native thermonuclear fusion significance [9] yielding no neutron output, and immersed in a dense plasma surrounding with $n_e = 10^{25}$ e-cm^{-3} and T(eV) = 500, 1000, and 2000. An immediate inspection of Fig. 6 demonstrates that the highest charge and heaviest B_{11}^{5+} BIM component provides, at all α values, the overwhelming stopping contribution when the target is submitted to low velocity proton beams. So, in the present situation, the target proton LVISD may be safely neglected when contrasted to that of B_{11}^{5+} and the electrons.

B. Astrophysical BIM

We now turn attention to two BIM of very important astrophysical pertinence, He^{2+}-C^{6+} featuring white dwarfs (WD) crust [10] and Si^{14+}-Sn^{36+} relevant to ion interdiffusion issues in stellar envelopes [11]. Both BIM feature a charge ratio $2.5 \leq Z_2/Z_1 \leq 3$ and mass ratio $M_2/M_1 \sim 3$, in dense plasmas with IFE-like parameters. Considering first, He^{2+}-C^{6+}, associated to the "carbon pollution" issue in WD, one has $n_e = 10^{26}$ e-cm^{-3} with T(keV) = 1, 2, and 5 (see Fig. 7), which as the above proton-, B_{11}^{5+} BIM advocates that C^{6+} dominates LVISD, at any relative proportion for $T \leq 2$ keV, when the target is exposed to incoming protons. In Fig. 7, V_p is measured in V_{th1} for $\alpha \leq 0.5$, and in V_{th2} for $\alpha \geq 0.5$. Both scalings are compared in
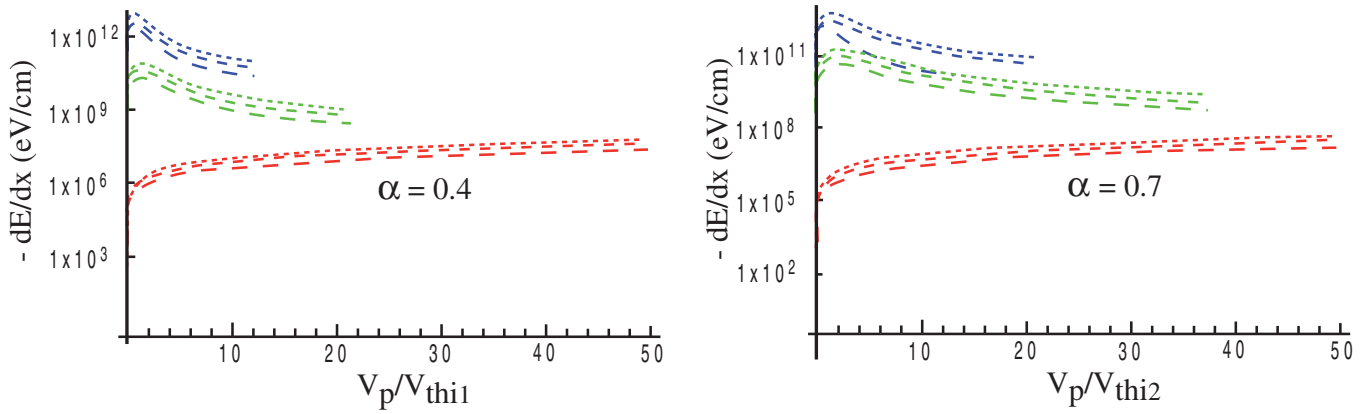
FIG. 7. (Color) Proton $-dE/dx$ (eV/cm) with respect to V_p/V_{thi} in a He^{2+}-C^{6+} BIM at $n_e = 10^{26}$ e cm^{-3} with $T(keV) = $ ($\cdots\cdots$) 1, ($-\cdot-\cdot-\cdot$) 2, and ($-$ $-$ $-$ $\cdot$) 5. $\alpha = He^{2+}$ concentration. Dark gray (red) denotes e stopping, light gray (green) pertains to He^{2+} stopping, and black (blue) to C^{6+} stopping.

Fig. 8 for $\alpha = 0.5$. As above, the electron LVISD does not show up on these very low velocity linear scales, while the He^{2+} contribution hardly appears when V_p is scaled by V_{thi2}.

Turning to Si^{14+}-Sn^{36} BIM immersed also in a dense plasma impacting α particles and advocated $n_e(cm^{-3}) = 10^{26}$ and $T(keV) = 100$ and 200, with pertaining to LVISD pictured on Figs. 9 with linear $-dE/dx(eV/cm)$. Within

the very low V_p/V_{thi} considered range, electron contribution has vanished and the Si^{14} one should be quantitatively included only for $\alpha = 0.9$ and $V_p/V_{th2} \gtrsim 4$. It should be recalled that in Fig. 9 as well as in many previous ones, we intend to contrast LVISD through the $\alpha \Leftrightarrow 1-\alpha$ exchange, and so depart to a certain extent from the usual increasing α monotone presentation.
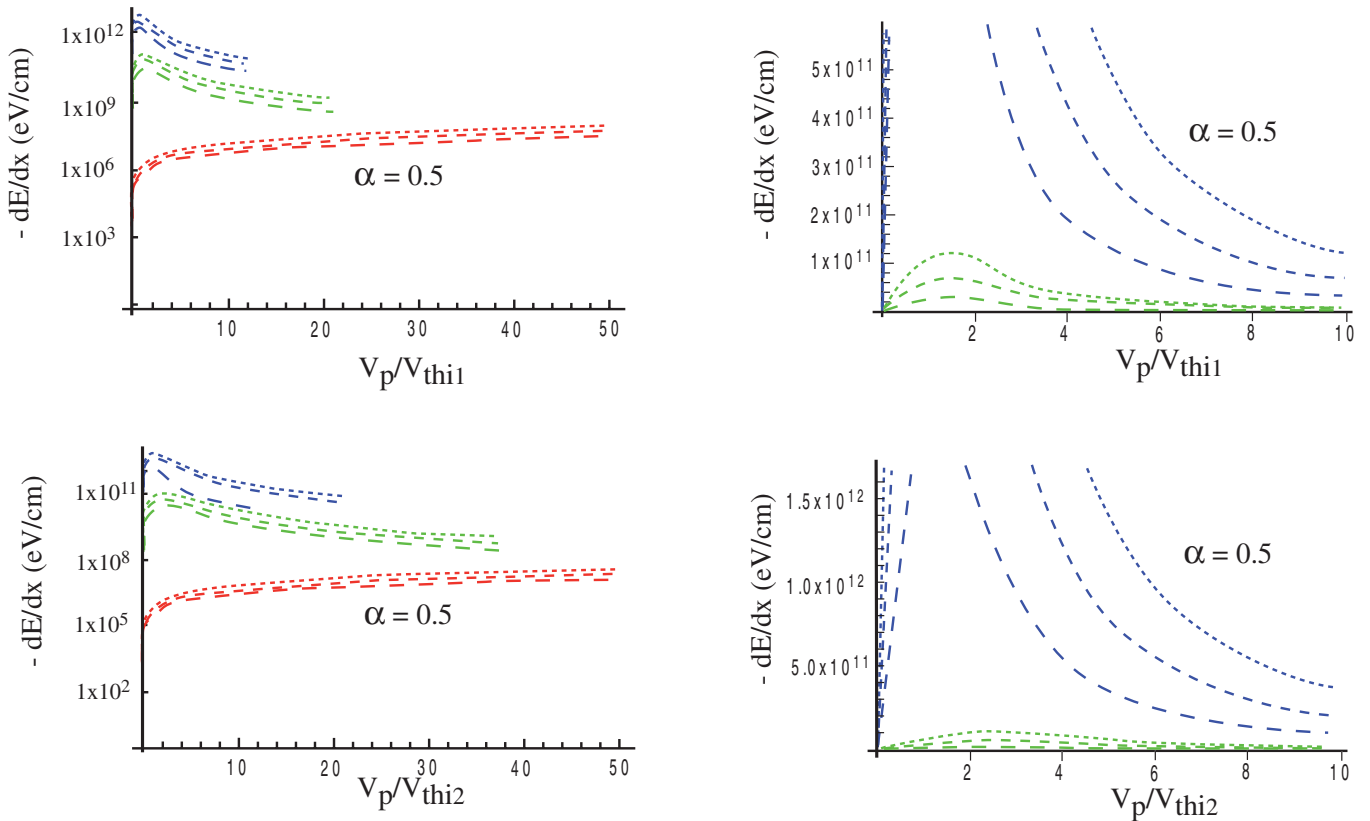

FIG. 8. (Color) Proton $-dE/dx$ (eV/cm) with respect to V_p/V_{thi} in a He^{2+}-C^{6+} BIM at $n_e = 10^{26}$ e cm^{-3} with $T(keV) = $ ($\cdots\cdots\cdots$) 1, ($-$ $-$ $-$ $-$ $-$) 2 ($-$ $-$ $-$ $-$) 5. $\alpha = He^{2+}$ concentration. Dark gray (red) denotes e stopping, light gray (green) pertains to He^{2+} stopping, and black (blue) to C^{6+} stopping.
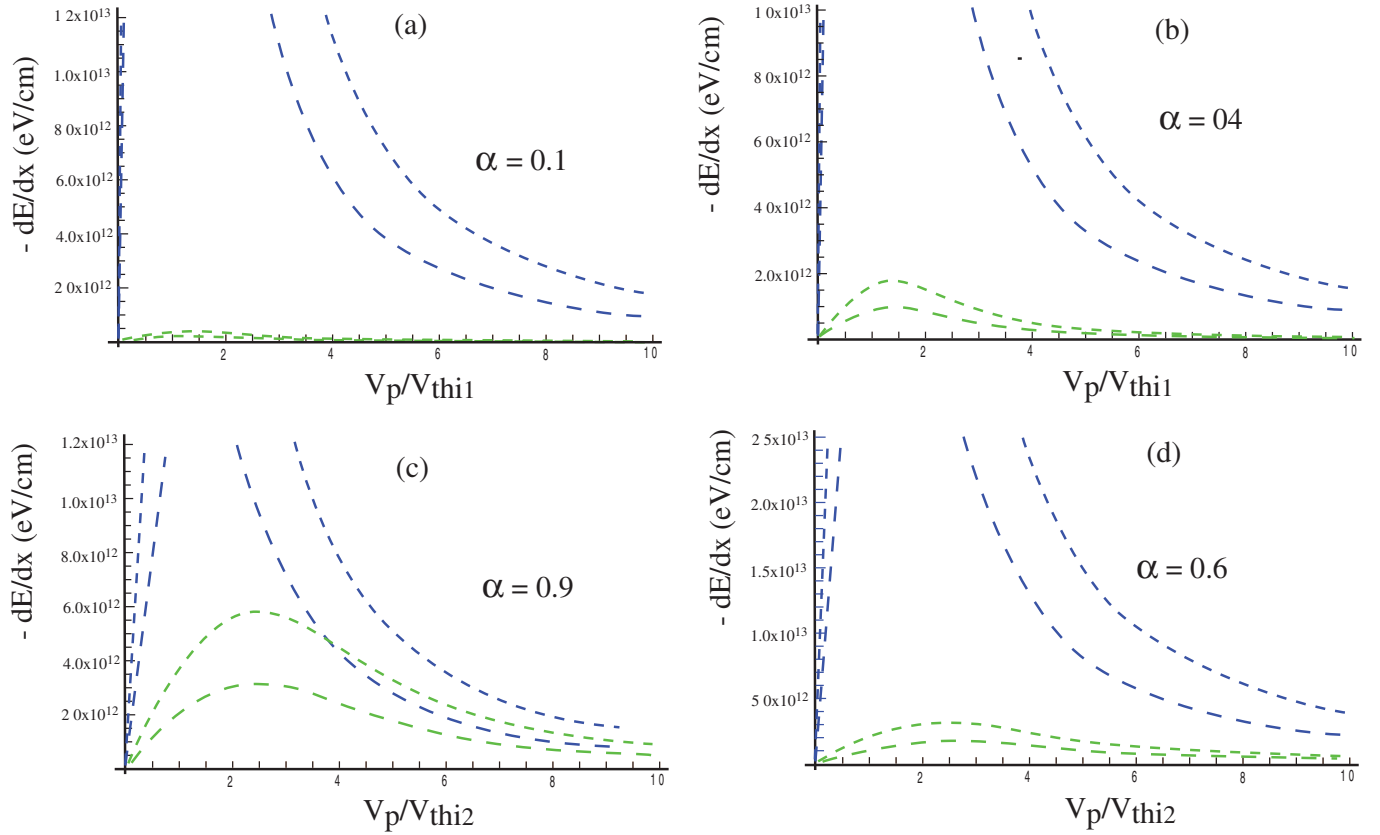
FIG. 9. (Color) Alpha particle projectile in a Si^{14+}-Sr^{36+} BIM with a $n_e = 10^{26}$ e cm^{-3} and temperatures = (– – – – – ·) 100 keV, (– – – –) 200 keV with Si^{14+} relative proportion: (a) $\alpha = 0.1$, (b) $\alpha = 0.4$, (c) $\alpha = 0.9$, and (d) $\alpha = 0.6$. Dark gray (red) refers to electron stopping, light gray (green) to D^+ stopping, and black (blue) denotes T^+ stopping, $-dE/dx$ (eV/cm) in terms of V_p/V_{thi}.

VI. PBAR-D^+ ($Z_2/Z_1 = -1$, $M_2/M_1 = 2$)

If one pushes the BIM charge dissymmetry up to including negatively charged ions, one reaches novel LVISD behaviors as displayed in Fig. 4 by the antiproton (pbar)-D^+ mixture submitted to He^{2+} projectiles. In contradiction to the previous patterns (Figs. 6–9), one now witnesses a rather well approximated quasisymmetry between $\alpha = 0.4$ and $\alpha = 0.6$ (see Fig. 10). The conspicuous feature now arises at $\alpha = 0.5$, when the two target ion LVISD exactly compensate each other, leaving only a much reduced electron stopping, within the given overall charge neutral target BIM.

The slight remaining asymmetric discrepancy arises from the mass ratio $M_2/M_1 = 2$ rendering D^+ a little less mobile than the pbar in a dense and hot plasma [$n_e = 10^{23}$ e-cm^{-3} with $T(\text{keV}) = 0.1$ and 1]. So the α-pbar attraction results in a noticeable larger LVISD at $\alpha = 0.6$ compared to that for deuton stopping at $\alpha = 0.4$.

VII. SUMMARIES AND OUTLOOK

As a first conclusive remark, we can notice that Eq. (11) usually fits rather well the linearly rising part of the LVISD curves.

The rather detailed exploration of low velocity ion stopping in several BIM of potentially high interest in thermonuclear fusion and astrophysics should allow a novel reinvestigation of the nuclear reaction rates at work in these systems. Moreover, the present dielectric formulation albeit restricted to a dense and classical electron fluid, could be easily extended to partially Fermi degenerate situations of obvious practical interest, by introducing the corresponding $\hbar \neq 0$ Fried-Conte extension [12,13].

In this regard, the matching of LVISD in these targets with an estimate of low ion velocity multiple scattering would also be of high interest [14].

In these regards, the ion projectile scattering probability writes as [14]

$$\frac{dP}{dq_\perp} = V_p \times G_{\forall\,T}(q_\perp), \qquad (12)$$

where

$$G_{\forall\,T}(q_\perp) = \frac{4Z^2 e^4 m_e^2}{\hbar^4 \pi} q_\perp \int_{q_\perp}^{\infty} \frac{1}{(q^2 + q_s^2)^2}$$

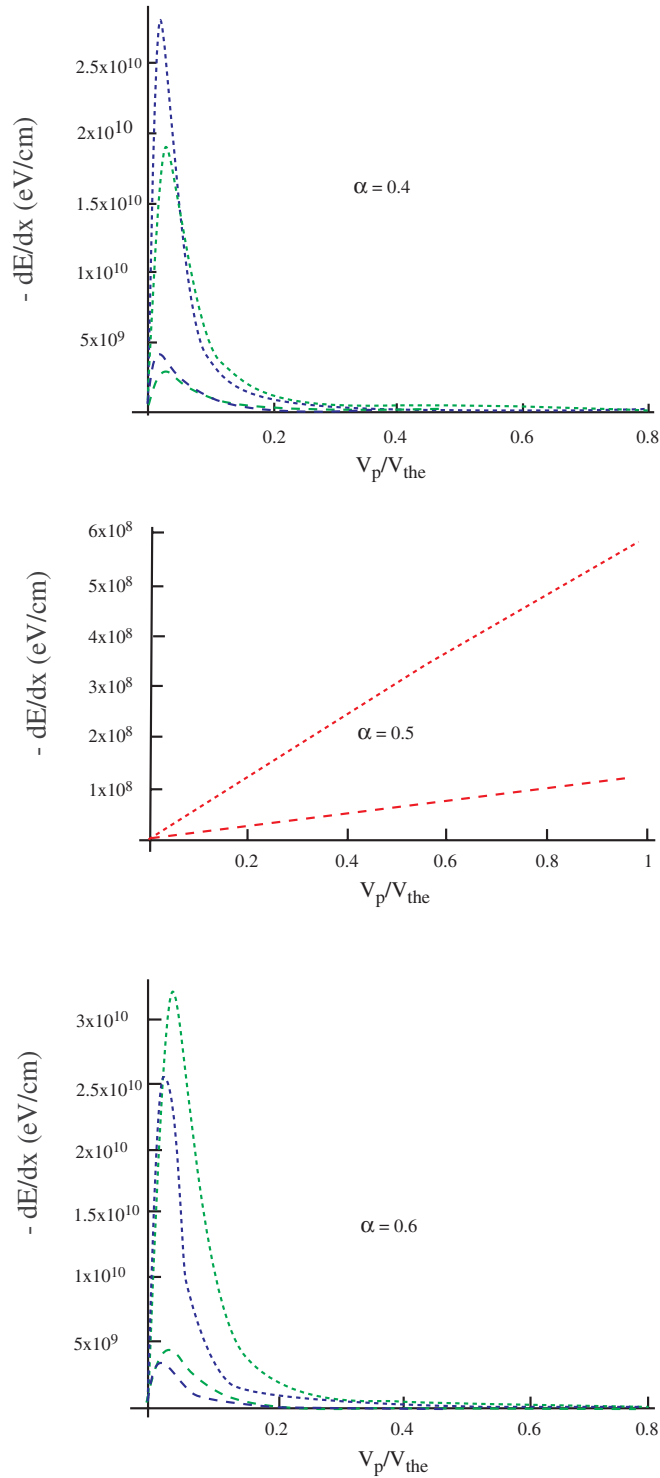$$\times \frac{1}{1 + \exp(\frac{\hbar^2}{8m_e T} q^2 - \eta)} dq \qquad (13)$$

FROMY, TASHEV, AND DEUTSCH

Phys. Rev. ST Accel. Beams **13**, 101302 (2010)

FIG. 10. (Color) He^{2+} $-dE/dx$ (eV/cm) in terms of V_p/V_{the} in a pbar-D^+ BIM with total ion density $= 10^{23}$ e cm^{-3}. α denotes relative pbar concentration. Dark gray (red) refers to e stopping light gray (green) to pbar stopping, and black (blue) H^+ stopping. TeV $=$ (·············) 100, and (- - - - - -) 1000.

with $q_\perp$, transverse projectile (charge Z) momentum, while q_s^2 qualifies target electron density and temperature with the usual $\eta = \beta_\mu$ normalized chemical potential.

Equation (12) advocates the V_p-linear dependence already featuring LVISD. However, the projectile-target mechanisms are markedly distinct, LVISD is monitored by target ion stopping, while present multiple scattering is essentially operated by target electrons.

Finally, inclusion of dynamical intrabeam correlations should document a realistic ion beam-plasma interaction at low velocity [15].

Starting with the charge quasisymmetric DT BIM, one perceives the charge asymmetry as an organizing concept in the data analysis.

ACKNOWLEDGMENTS

[1] P. Sigmund and A. Schinner, Nucl. Instrum. Methods Phys. Res., Sect. B **195**, 64 (2002).

[2] G. Logan, F. Bieniosek, C. Celata, E. Henestroza, J. Kwan, E. P. Lee, M. Leitner, L. Prost, P. Roy, P. A. Seidl, S. Eylon, J. L. Vay, W. Aldron, S. Hu, J. Barbard, D. Callahan, R. Cohen, A. Friedman, D. Grote, M. K. Covo, W. R. Meier, A. Molvik, S. Lund, R. Davidson, P. Efthimion, E. Gilson, L. Grisham, I. Kaganovich, H. Qin, E. Startsev, D. Rose, D. Welch, C. Olson, R. Kishek, P. O'Shea, and I. Haber, Nucl. Instrum. Methods Phys. Res., Sect. A **544**, 1 (2005).

[3] L. S. Grisham, Phys. Plasmas **11**, 5727 (2004).

[4] G. Zwicknagel, C. Toepffer, and P.-G. Reinard, Phys. Rep. **309**, 117 (1999).

[5] B. D. Fried and S. D. Conte, *The Plasma Dispersion Function* (Academic Press, New York, 1961).

[6] C. Deutsch, Ann. Phys. (Paris) **11**, 1 (1986); C. Deutsch and G. Maynard, Recent Res. Dev. Plasmas **1**, 1 (2000).

[7] Th. Peter and J. Meyer-ter-Vehn, Phys. Rev. A **43**, 1998 (1991).

[8] M. Tabak, J. Hammer, M. E. Glinsky, W. L. Kruer, S. C. Wilks, J. Woodworth, E. M. Campbell, M. D. Perry, and R. J. Mason, Phys. Plasmas **1**, 1626 (1994); C. Deutsch, Eur. Phys. J. Appl. Phys. **24**, 95 (2003).

[9] D. C. Moreau, Nucl. Fusion **17**, 13 (1977); S. Eliezer and J. M. Martinez-Val, Laser Part. Beams **16**, 581 (1998).

[10] See, for instance, L. Siess, Astron. Astrophys. **448**, 717 (2006).

[11] D. B. Boercker and E. L. Pollock, Phys. Rev. A **36**, 1779 (1987).

[12] C. Deutsch, Phys. Lett. **60A**, 317 (1977); N. R. Arista and W. Brandt, Phys. Rev. A **29**, 1471 (1984).

[13] C. Gouedard and C. Deutsch, J. Math. Phys. (N.Y.) **19**, 32 (1978); R. G. Dandrea, N. W. Ascroft, and A. E. Carlsson, Phys. Rev. B **34**, 2097 (1986).

[14] R. Popoff, G. Maynard, and C. Deutsch, Phys. Rev. E **80**, 046408 (2009).

[15] C. Deutsch and N. A. Tahir, Phys. Fluids B **4**, 3735 (1992).